# Large-scale fabrication of three-dimensional scaffold-based patterns of microparticles and breast cancer cells using reusable acoustofluidic device

Tan Dai Nguyen[a], Van-Thai Tran[a], Sanam Pudasaini[a], Archana Gautam[a], Jia Min Lee[a], Yong Qing Fu[b], Hejun Du[a,*]

[a] School of Mechanical and Aerospace Engineering, Nanyang Technological University, 639798, Singapore

[b] Faculty of Engineering and Environment, Northumbria University, Newcastle upon Tyne, NE1 8ST, UK

## Abstract:

Spatial distribution of biological cells plays a key role in tissue engineering for reconstituting the cellular microenvironment, and recently acoustofluidics have been explored as a viable tool for controlling structures in tissue fabrication because of its good biocompatibility, low-power consumption, automation capability, nature of non-invasive and non-contact. Herein, we developed a reusable acoustofluidic device using surface acoustic waves for manipulating microparticles/cells to form a three-dimensional (3D) matrix pattern inside a scaffold-based hydrogel contained in a millimetric chamber. The 3D patterned and polymerized hydrogel construct can be easily and safely removed from the chamber using a proposed lifting technique, which prevent any physical damages or contaminations and promote the reusability of the chamber. The generated 3D patterns of microparticles and cells were numerically studied using finite element method, which was well validated by the experimental results. Our proposed acoustofluidic device is a useful tool for *in vitro* engineering three-dimensional scaffold-based artificial tissues for drug and toxicity testing and building organs-on-chip applications.

**Keywords**: surface acoustic waves, acoustofluidics, microfluidics, 3D patterning, organs-on-chips

---

* Authors to whom correspondence should be addressed: MHDU@ntu.edu.sg

## 1. Introduction

Tissue engineering is an interdisciplinary field which utilizes biotechnology and engineering to develop artificial tissues [1, 2]. State of the art techniques in tissue engineering have recently been hindered by some fundamental problems of maintaining viability, function and structure, while achieving more accurate patterning architectures that similar to architectures of tissues [2]. In scaffold-based tissue engineering, cells are seeded onto three-dimensional (3D) scaffolds that provide a temporary 3D environment, and mechanical support for tissue growth [3-5]. Cells in the tissues are highly sensitive to geometrical and mechanical cues from their microenvironment [6-8]. Geometries in the microenvironment such as the position and orientation of adjacent cells, cells density and their distributions play an important role on cellular physiology, from intracellular organization to multicellular morphogenesis [9]. For example, the lack of organized elastin in vascular grafts contributes to multiple failure mechanisms [10]. In microfabrication, micropatterning techniques offer excellent control for engineering of 3D structures of cells in tissue engineering scaffold [6, 11, 12]. Therefore, many techniques have been developed to achieve the patterning of cells in the microenvironment from mesoscale, e.g., using cell sheet, cell-laden hydrogel and 3D printing; to microscale e.g., microfluidics, using electrical stimulation, optical guiding, inkjet-based cell printing, and laser-assisted printing [1, 9]. Among several approaches to achieve this, the acoustic-based methods, especially surface acoustic waves (SAWs), has been rapidly developed as a fast, non-invasive, biocompatible and contactless technique for manipulating and patterning of cells in microfluidic channels [13-25]. The current designs of SAW devices require direct bonding of chamber on a piezoelectric substrate which may causes cross-contamination, cell loss and structure deformation. To overcome this issue, a reusable acoustic tweezers for disposable SAW device by introducing a coupling liquid layer between a removable, independent

polydimethylsiloxane (PDMS)-glass hybridized microfluidic chamber and the device. The transmission of acoustic waves from lithium niobite substrate into a superstrate has been reported [26-29]. Although there is a reflection of the longitudinal wave at interfaces of glass/liquid and lithium niobate/liquid, the transmission of acoustic power into the superstrate is still sufficient to generate a Lamb wave [27]. This set-up has been applied for various lab on a chip applications such as droplet manipulations, [30-34] and particle enrichment [35, 36]. In addition, we have previously shown that SAW devices are capable of patterning polymer microparticles into three-dimensional matrix structures [15, 37], as well as precisely and reliably controlling the 3D position of single microparticles and cells [38]. However, to date, no studies have explored the use of the reusable SAW or acoustofluidic device for rapid 3D patterning of biological objects in scaffold-based hydrogels contained in a millimeter-scale microfluidic chamber.

In this study, we developed a reusable acoustofluidic device for manipulating microparticles and biological cells into 3D matrix pattern in a scaffold-based collagen hydrogel using SAWs. Type I collagen was used as the hydrogel scaffold owing to its popularity, ease of extraction and adaptability [39, 40]. The rapid gelation of type I collagen is also suitable for restricting the movement ability of 3D patterned structures. This hydrogel has been found widespread use in 3D scaffold-based culture in tissue engineering, especially in 3D bioprinting [40-43]. In this reusable acoustofluidic device, microparticles and cells are manipulated to form a 3D pattern in the collagen hydrogel that looks like crystal-like structure. The 5 mm × 5 mm × 5 mm open-top chamber has a capacity to contain the hydrogel solution up to 0.125 ml and can be scaled to larger dimension (e.g. centimeter-scale). For the purpose of reusability, removal of the chamber from the SAW device was achieved by using the coupling liquid for guiding acoustic waves from the device to the chamber [26], while removal of the 3D polymerized, patterned hydrogel construct by employing a buoyant force lifting technique. Using this way, the

hydrogel construct could be easily and safely removed from both chamber and device, along with preventing any external physical damages and contaminations. Our developed device is highly suitable for *in vitro* engineering 3D artificial tissues or integrating into organ-on-chip platforms.

## 2. Method

### 2.1. Device fabrication

SAW device was fabricated by depositing the interdigital transducers (IDTs) which were made of metal electrodes (Cr/Au, 10 nm/50 nm) on a 128° Y-cut lithium niobate ($LiNbO_3$) substrate using standard photolithography and lift-off processes. The IDTs consisted of 40 pairs of fingers with both width and space gap of 75 µm, corresponding to the SAW wavelength of 300 µm. A 5 mm × 5 mm × 5 mm (length × width × height) PDMS chamber (Sylgard 184 Silicone Elastomer; Dow Corning, USA) was prepared using a soft casting method into a custom aluminum mold. A cover glass (22 mm wide × 22 mm long × 0.15 mm thick) was then attached to the bottom of the chamber to form an open-top PDMS-glass chamber or an open-top superstrate [26, 27]. The chamber has an open-top face that promotes penetration of culture medium into the cell-hydrogel construct and for easily removal of gelled hydrogel construct.

### 2.2. Preparation of biological cells and microparticles

Michigan Cancer Foundation-7 (MCF-7) breast cancer cell line, purchased from the American Type Culture Collection, were cultured in Dulbecco's Modified Eagle Medium (Gibco; Thermo Fisher Scientific, USA), supplemented with 10% FBS and 1% antibiotic. The cells were maintained to grow in an incubator (HERACELL VIOS 160i, Thermo Fisher Scientific, USA) at 37°C and 5% $CO_2$ for three to four days until 70 to 80% confluence was reached. They were then trypsinized using 0.05% trypsin and collected by centrifuging at 250

g for 5 mins. The cell pellet was re-suspended in complete media and counted using a hemocytometer. The final concentration was adjusted to $4.68 \times 10^6$ cells/ml for the experiments.

Two types of microparticle were used in the experiment i.e., non-functionalized polystyrene microspheres (average size of 10 µm, concentration of $4.55 \times 10^7$ microparticles/ml, Polysciences, USA), and fluorescent polystyrene microspheres (average size of 10 µm, concentration of $1 \times 10^6$ microparticles/ml, Thermo Fisher Scientific, USA).

### 2.3. Live/dead viability assay

The cells were stained with the commercially available LIVE/DEAD™ Cell Imaging Kit (Invitrogen™ by Thermo Fisher Scientific, USA). According to the manufacturer, Live Green was mixed with the Dead Red and 1 mL of the mixture was added on the cell-hydrogel construct. The construct was incubated for 30 mins at room temperature before being imaged with a fluorescence microscope (Eclipse Ti-U, Nikon, Japan). The viability of the cells was determined by counting the number of live and dead cells from captured fluorescent images.

### 2.4. Preparation of collagen solution

Corning® Collagen, rat tail Type I (4.88 mg/ml, Corning Inc, USA) was used according to the manufacturer's protocol. The collagen was diluted with 10X Phosphate-Buffered Saline (PBS) and Deionized (DI) water. The mixture was then neutralized by adding 1N Sodium Hydroxide (NaOH), making the final volume 0.5 ml. This was quickly followed by the addition of 0.5 ml cell suspension and Live/Dead solution. The final cell concentration of cell and collagen was $1.15 \times 10^6$ cells/ml and 0.815 mg/ml, respectively.

## 2.5. Numerical method

Patterning behavior of the mixed solution of collagen and microparticles within the chamber was simulated. The numerical model was simplified to a two-dimensional rectangular domain that viewed from the right side [15]. The simulation model simply solves the Helmholtz's equations [44], together with the boundary conditions using the finite element method integrated into the COMSOL software to obtain the first order acoustic pressure and the acoustic radiation potential.

## 2.6. Experimental set up

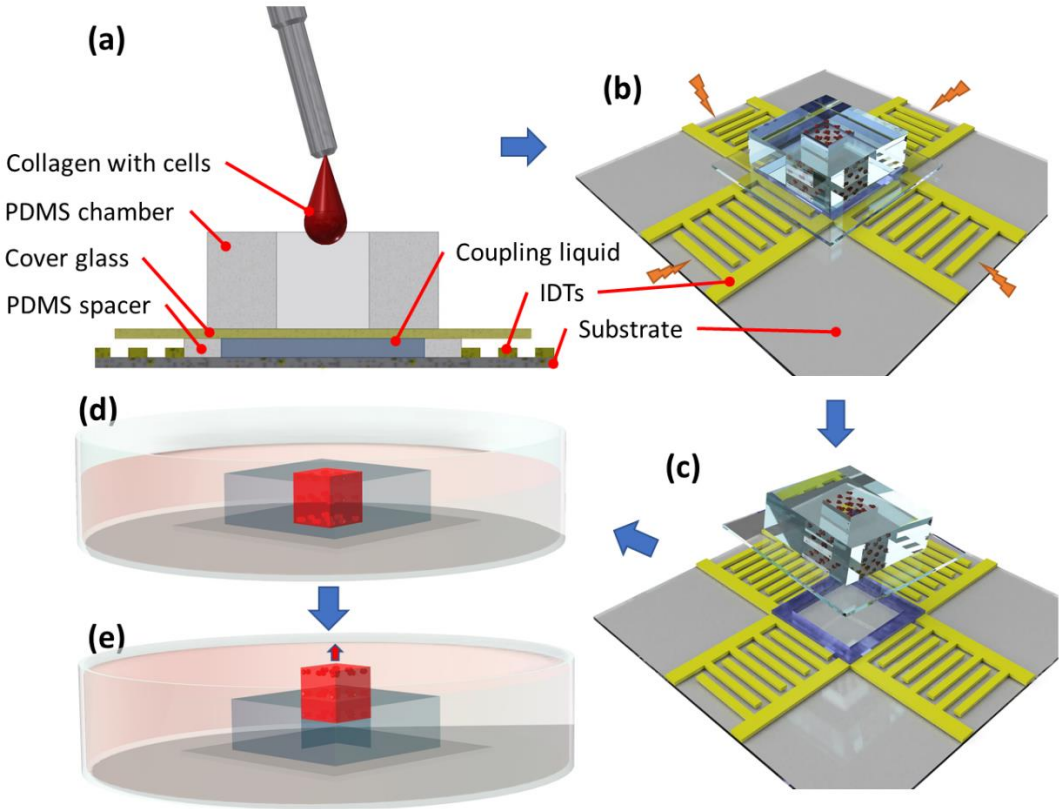


**Figure 1** The schematic diagram of experimental setup and procedures. (a) A mixed solution of hydrogel and cells was injected into an open-top PDMS-glass chamber, which was previously placed on the SAW device with a coupling liquid at the gap between the chamber and the device. A PDMS spacer was used to create space for containing the coupling liquid and

preventing it from leakage (b) The IDTs of SAW device were powered to perform 3D patterning. (c) The chamber was taken off from SAW device. (d) The chamber was transferred to a petri dish containing culture medium. (e) The 3D polymerized, patterned hydrogel construct was removed from the chamber by dipping the entire chamber into the medium, which based on buoyant force lifting principle.

The experimental setup and procedures are illustrated in **Figure 1**. Prior to the experiments, the open-top PDMS-glass chambers were sterilized with 70 % ethanol solution for 2 hours and then rinsed with Deionized (DI) water. The chamber was then placed on the SAW device with the coupling liquid as shown in **Figure 1**a. The coupling liquid was used as an acoustic guide for transmitting the acoustic waves from SAW device to the chamber [26]. A PDMS spacer was used to create a gap for the coupling liquid while preventing the liquid leaks. The chosen coupling liquid was 70% ethanol solution due to its low acoustic impedance, availability and easy cleaning. A mixed solution of collagen and microparticles/cells was then injected into the chamber (**Figure 1**a). Then, the SAW device was powered to perform 3D patterning of microparticles/cells in collagen solution (**Figure 1**b). When the hydrogel was partially polymerized after about 10 mins, the open-top PDMS-glass chamber was removed from the device (**Figure 1**c) for imaging using fluorescence microscopy or for culturing in the incubator (**Figure 1**d). The 3D polymerized, patterned hydrogel was removed from chamber by dipping the entire chamber into a petri dish that contained medium liquid and letting the buoyant force to lift it up (**Figure 1**d, e). Cell viability was evaluated after patterning for 1 hour and 24 hours.

## 3. Results and discussion

### 3.1. 3D patterns of microparticles in collagen hydrogel

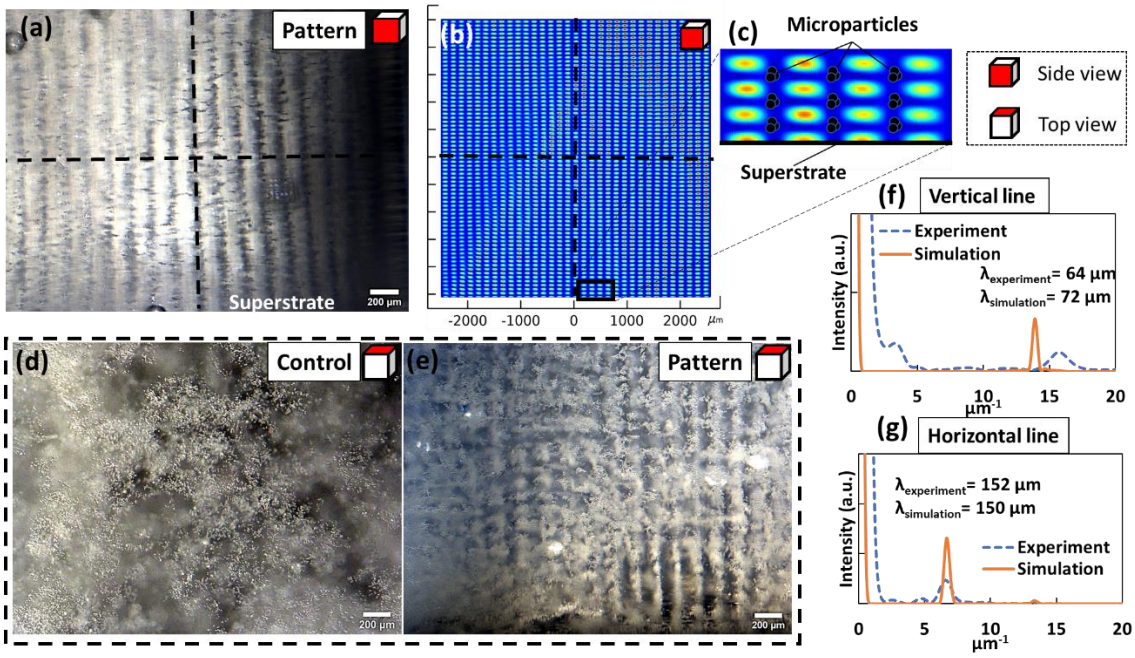


**Figure 2** Side views of (a) experimental pattern sample (scale bar: 200 μm) and (b) simulated acoustic radiation potential. (c) Enlarged image of acoustic radiation potential and locations where microparticles can be trapped. (d) and (e) are top views of control and pattern samples, respectively (scale bar: 200 μm). (f) and (g) are 1D Fast Fourier transform (FFT) along the vertical and horizontal dashed lines, respectively,that displayed in Figure 2(a) and (b).

The simulation model was first used to calculate the acoustic pressure field where the highest and lowest acoustic pressure areas are alternatively distributed in 2D plane (**Figure S5** in Supporting Information). This result was then employed to calculate acoustic potential field (**Figure 2**b). The acoustic potential field explains the potential of the acoustic radiation force. In the acoustic potential field, the acoustic radiation force is directed from the high-value potential positions to low-value potential positions in three-dimensional space. Under this

force, the microparticles were relocated to the lowest potential positions (i.e., pressure node positions) as shown in enlarged image of **Figure 2**b. By simulating the acoustic pressure and the acoustic potential field within the chamber, the formation of microparticles into a 3D pattern inside the hydrogel can be confirmed. To verify the simulation results, experiments on SAW device were conducted to perform 3D patterning of polystyrene microparticles with diameter of 10 μm in the collagen solution at a power of 24.85 dBm. Two samples with the same volume of mixed solution of collagen and microparticles were prepared. One was placed on the SAW device for generating 3D patterns and the other was left freely as a control sample for comparison. After 10 minutes, both samples were polymerized. **Figure 2**d and **2e** are optical microscopic images that show the top views of these two samples. Microparticles in the pattern sample has regular distribution along two directions (i.e. vertical and horizontal directions). Meanwhile, microparticles in the control sample has a random distribution. **Figure 2**a shows the side view of the pattern sample which has the similar pattern to the simulation result as shown in **Figure 2**b. In this experiment, an optical prism was applied to enable the side view [15]. In structural organization of tissues, especially, patterning structure, spacing between pressure nodes (i.e. trapped microparticles/cells) is the most important factor [45]. Therefore, we have determined spacing of the 3D patterns from **Figure 2**a and **2**b by applying Fast Fourier transform (FFT). **Figure 2**f and **2**g show the FFT for the directions along the vertical and horizontal dashed lines, respectively, that displayed in **Figure 2**(a) and **2** (b). The results show that the periodic spacing (half-wavelength) of the pattern along horizontal dashed line are similar between experiment and simulation. Meanwhile, the periodic spacing along vertical dashed line from simulation is higher than that in experiment. The reason for this difference might be caused by the overlap of microparticles of two adjacent nodes. Another experiment was conducted using fluorescent microparticles that enables better vision will be presented in

**Figure 4**. From the top and side views of pattern sample, it can be concluded that the microparticles have been assembled into a 3D pattern.

The formation mechanism of 3D pattern was thoroughly investigated in our previous publication but with a smaller chamber (i.e., 1 mm in height) and PDMS top cover [15]. The results were similar between the patterns in a 1 mm chamber and a 5 mm chamber in terms of the distribution of nodes and the distances between the nodes. It could be noted that the 3D patterns could be achieved even on a larger-scale chambers, which show the capability of engineering large-size artificial tissues. The patterning structure, however, is not uniform at some areas due to various reasons including the effect of second-order acoustic streaming, variation of temperature along the depth since the heat source is from superstrate, the shrinkage of hydrogel after polymerization, discrepancy of standing Lamb waves and deformation of top free fluid surface. The open top surface helps on the removal of gelled construct and promote the penetration of nutrient medium to the cells. We have tested the deformation of free fluid surface at different power values (**Figure S3**). Thereby, the deformation of top free fluid surface is tiny for power of 24.85 dBm which was used in experiments.

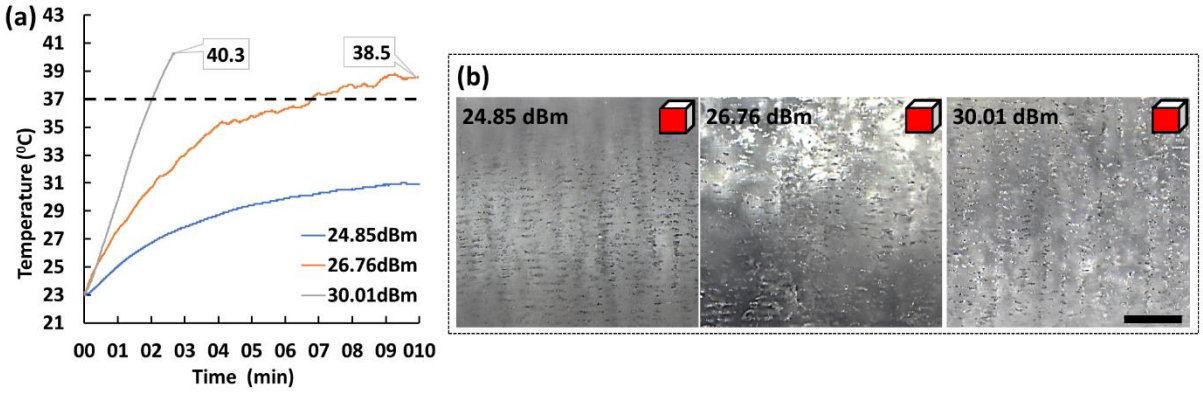


**Figure 3** (a) Measured temperature of the mixed solution of collagen and microparticles for 10 minutes at the power 24.85 dBm, 26.76 dBm and 30.01 dBm. (b) Patterned formations at the power of 24.85 dBm, 26.76 dBm and 30.01 dBm, respectively.

The collagen type I forms a firm gel at the neutral pH value and a temperature of 37 $^{o}$C [46]. In our experiment, once its pH is neutralized, the collagen solution can be polymerized when its temperature is increased due to the heat generated from the IDTs of SAW device. This heat plays a fundamental role in facilitating the gelling process. Since the rate of temperature increase is highly influenced by the applied power of SAW device, the control of chamber temperature is dependent on the control of the SAW power and time duration. At first, we investigated the temperature changes of the mixed solution of collagen and microparticles at different powers. **Figure 3**a shows the temperature changes at SAW powers of 24.85 dBm, 26.76 dBm, and 30.01 dBm for 10 minutes using a thermometer (t3000FC, Fluke, USA). It can be seen that the higher power resulted in a higher increasing rate of temperature. However, at the power of 26.76 dBm and 30.01 dBm, the temperature exceeded $37^{0}$C which may have some negative influences on the cell viability. Moreover, a rapid increase of fluid temperature could induce significant heat convection, thus resulting in convective fluidic flows. In addition, since the SAW-induced acoustic streaming velocity is proportional to the SAW power [47-53], higher powers can cause high-velocity acoustic streaming flows. These convective and acoustic streaming flows could lead to the deformation of 3D patterned structures before the polymerization occurred. The results in **Figure 3**b and **3**c show that the formation of 3D patterns after polymerization at different values of SAW power. At the SAW power of 24.85 dBm, 3D patterned structure was still maintained and fully polymerized while the 3D patterned structures at power of 26.76 dBm and 30.01 dBm were slightly deformed. After optimization, we identified the suitable power value and duration to get the best performance were 24.85 dBm and 10 minutes, respectively. Because at this power, the solution temperature was keeping below $37^{0}$C for preventing damage of the cells. To improve performance of the next-gen devices, the solution temperature should be controlled by modulating drive of the SAW, because the difference in the hydrodynamic and acoustic time scales permits one to run the

SAW device with a much decreased duty cycle to facilitate similar hydrodynamic phenomena while at much less total acoustically driven heating [54].

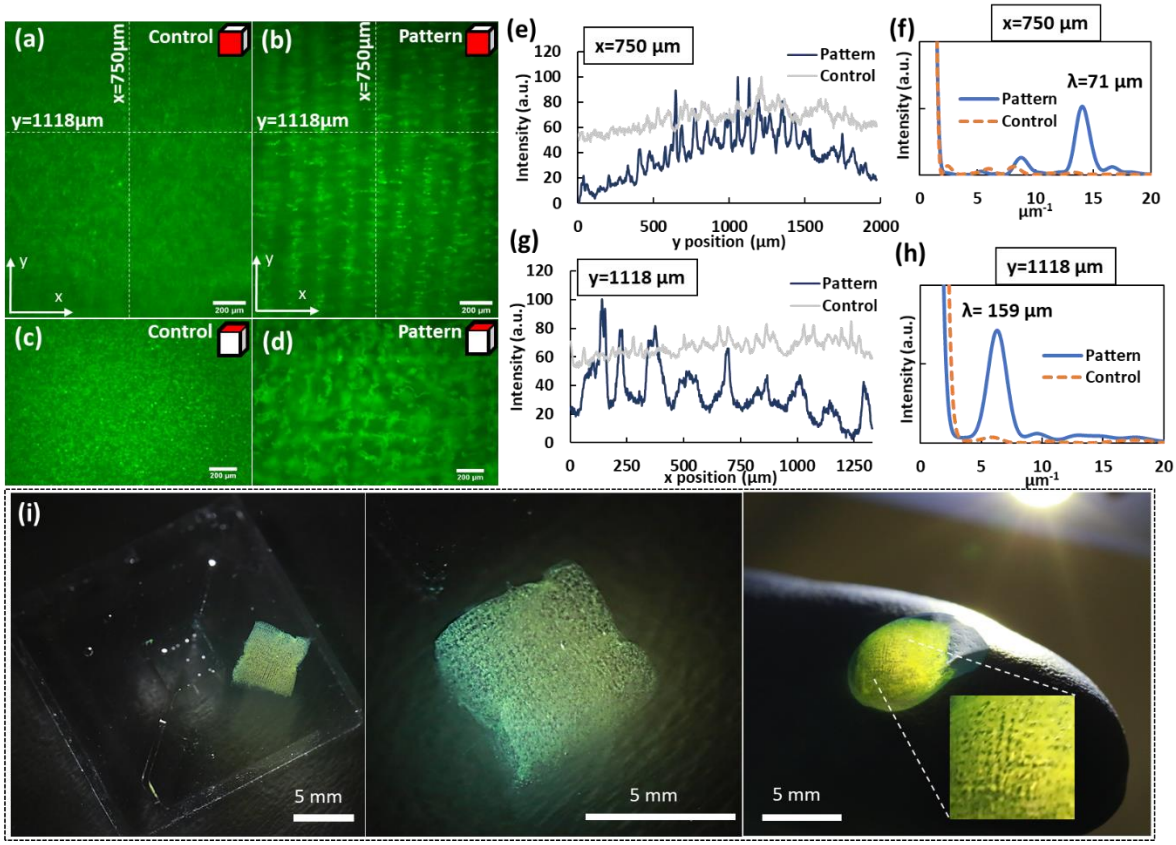


**Figure 4** Side views (a and b) and top views (c and d) of the control sample (a and c) and pattern sample (b and d), respectively (scale bar: 200 µm). (e) and (f) are intensity analysis and 1D FFT along the lines at x = 750 µm of both control and pattern samples, respectively. (g) and (h) are intensity analysis and 1D FFT along the lines at y = 1118 µm of both control and pattern samples, respectively. The intensity value ranges from 0 (minimum) to 255 (maximum). (g) Removal of patterned hydrogel from the chamber. From left to right: the hydrogel construct was placed onto the chamber in DI water after removal, a closer view of the removed hydrogel construct with clear patterned structure, and the hydrogel construct was placed on a finger when still maintained the patterned structure (scale bar: 5 mm).

When the mixed solution of fluorescent microparticles and collagen solution is patterned and polymerized completely, the fluorescent images can reveal the accumulation positions of microparticles (i.e., positions of pressure nodes) based on the peak of fluorescent intensity. **Figure 4**a to **4**d show the fluorescent images from side and top views of both pattern and control samples. Meanwhile, **Figure 4**e and **4**g show the graphs of fluorescent intensity variations along the vertical lines crossing pressure nodes (i.e., x = 750 μm) and along horizontal lines crossing pressure nodes (i.e., y = 1118 μm) of two samples. For the pattern sample, the intensity along have regular peaks distribution. The intra- and inter-layer distances of the pressure nodes were determined based on the periodic distribution of these peaks. An analysis using FFT for the directions along the lines x = 750 μm and y = 1118 μm are shown in **Figure 4**f and **4**h , respectively. Their results show the periodic separation between two nodes along vertical and horizontal directions are 71 μm and 159 μm, respectively. These values are close to those in simulation results presented in **Figure 2**f and **2**g (i.e. 72 μm and 150 μm, respectively). In comparison to the control sample, the intensity lines are randomly distributed without having regular peak distribution and the FFT analyses do not show any significant peaks.

After polymerization, it is necessary to remove the hydrogel from the open-top PDMS-glass chamber while ensuring the integrity of the 3D patterned structure. Herein, we proposed a removing technique based on buoyant force lifting principle, which is also known as Archimedes' principle. When the chamber was separated from SAW device and dipped into the medium (**Figure 1**d), the liquid medium leaked inside the chamber resulting in a buoyant force subjected to the hydrogel. Considering the gravity, since the density of hydrogel is slightly lower than the density of medium, the hydrogel was then under a net upward force, i.e., $F = Vg(\rho_M - \rho_H)$ where V is the hydrogel's volume, g is the gravitational acceleration,

$\rho_M = 1.000$ g/ml is the medium's density and $\rho_H = 0.991$ g/ml is the hydrogel's density. As a result, the hydrogel can be levitated and removed from the open-top PDMS-glass chamber to float into the medium. A spatula was used to assist separating parts of the hydrogel that stuck to the chamber walls. **Figure 4**g shows a 3D patterned hydrogel construct of fluorescent microparticles after being removed from chamber. After removal, the hydrogel construct could be collected by the spatula or by removing all the liquid medium out. This removing technique also helps to prevent any physical contacts or contaminations to the hydrogel construct, which may damage the 3D patterned structure.

### 3.2. 3D patterns of MCF7 cells in collagen

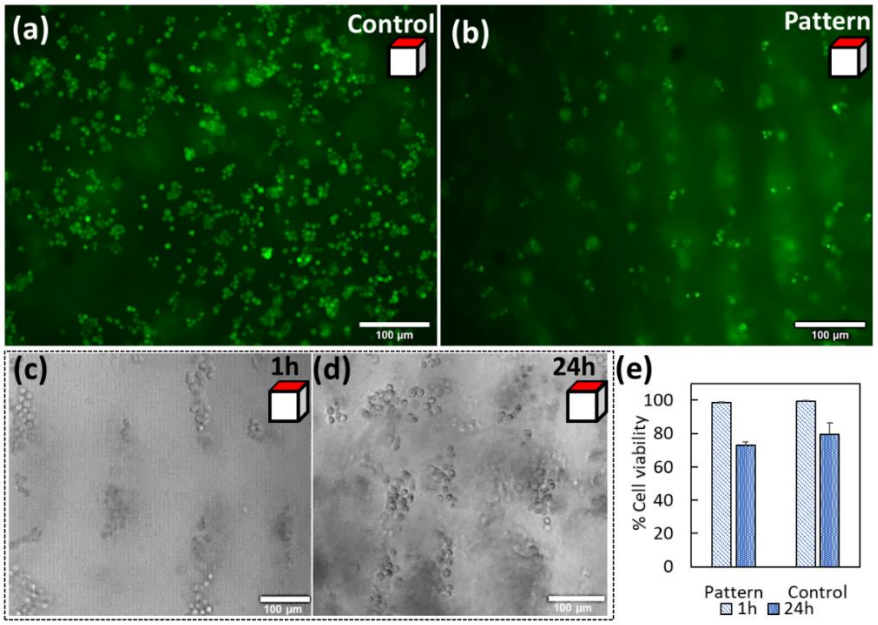


**Figure 5** (a) and (b) Top view of control and pattern samples of live cells after staining, respectively (scale bar: 100 µm). (c) and (d) Optical images of pattern sample after 1h and 24h, respectively (scale bar: 100 µm). (e) Quantitative analysis of the cell viability of control and pattern samples after 1h and 24h (plot as mean ± standard deviation).

We further performed 3D patterning of breast cancer cells in collagen hydrogel. The cells were stained and mixed with collagen solution before being injected into the chamber. Two samples were prepared, including one for patterning and one for control group. After patterning using the SAW device, both of the samples were taken for imaging under the fluorescent microscope. **Figure 5**a shows the top view of control sample where the cells are formed into clusters with random shapes and sizes. Whereas the pattern sample is shown in **Figure 5**b where most of clusters of cells were equally distributed. There are some faded clusters as they are located at other layers of the 3D pattern. The hydrogel construct was then cultured in the incubator for 24 hours to assess the cell viability. In **Figure 5**d and **5**e, we show the optical images of cells patterning in 3D patterned hydrogel construct at 1h and 24h, respectively. The cells are clearly aggregated at clusters which have a regular distribution. The decrease of both samples' viability is caused by the toxicity of Live/Dead solution. A few dead cells in the pattern sample may be attributed to the heat that transferred from the IDTs of SAW device. Moreover, there is no significant difference between the pattern and the control samples' viability at 1h and 24 h (*p-value* > 0.01, $p = 0.107$, Anova Two-Factor with Replication), which proves that the 3D patterning using SAW device does not significant affect the viability of the cells.

## 4. Conclusion

In this study, a reusable acoustofluidic device for constructing 3D scaffold-based patterns of microparticles and cells in hydrogel was reported. The polystyrene microparticles and breast cancer cells in collagen hydrogel were driven by the acoustic radiation force to form 3D patterns in an open-top PDMS-glass chamber before being polymerized. The formation mechanism of the 3D patterns was revealed from the simulation results which were in good agreement with experimental results. The chamber is connected with the piezoelectric substrate

of SAW device via a coupling liquid, which promotes the ease of assembling and removal of the chamber as well as the reusability of the SAW device. The 3D patterned, polymerized hydrogel could be removed from chamber by using a lifting buoyant force technique, which allows patterned construct in hydrogel to be further utilized. Therefore, this is useful tool for applications in engineering *in vitro* 3D scaffold-based artificial tissues, especially, for drug and toxicity testing and integrating into organs-on-chips platforms.

## 5. Acknowledgment

The authors gratefully acknowledge the support of (i) Nanyang Technological University and the Ministry of Education of Singapore through a PhD Scholarship and AcRF Tier 1 research grant (RG 96/18); (ii) the UK Engineering and Physical Sciences Research Council (EPSRC) grants (EP/P018998/1); (iii) Special Interesting Group of Acoustofluidics funded by UK Fluids Network (EP/N032861/1).

## 6. References

1. Khademhosseini, A., et al., *Microscale technologies for tissue engineering and biology.* Proceedings of the National Academy of Sciences of the United States of America, 2006. **103**(8): p. 2480-2487.
2. Berthiaume, F., T.J. Maguire, and M.L. Yarmush, *Tissue Engineering and Regenerative Medicine: History, Progress, and Challenges.* Annual Review of Chemical and Biomolecular Engineering, 2011. **2**(1): p. 403-430.
3. Khademhosseini, A. and R. Langer, *Microengineered hydrogels for tissue engineering.* Biomaterials, 2007. **28**(34): p. 5087-5092.
4. Kim, B.-S. and D.J. Mooney, *Development of biocompatible synthetic extracellular matrices for tissue engineering.* Trends in Biotechnology, 1998. **16**(5): p. 224-230.
5. Hutmacher, D.W., *Scaffold design and fabrication technologies for engineering tissues — state of the art and future perspectives.* Journal of Biomaterials Science, Polymer Edition, 2001. **12**(1): p. 107-124.
6. Théry, M., *Micropatterning as a tool to decipher cell morphogenesis and functions.* Journal of Cell Science, 2010. **123**(24): p. 4201-4213.
7. Tseng, Q., et al., *Spatial organization of the extracellular matrix regulates cell–cell junction positioning.* Proceedings of the National Academy of Sciences, 2012. **109**(5): p. 1506-1511.

8. Sala, A., et al., *Engineering 3D cell instructive microenvironments by rational assembly of artificial extracellular matrices and cell patterning.* Integrative Biology, 2011. **3**(11): p. 1102-1111.
9. Guillotin, B. and F. Guillemot, *Cell patterning technologies for organotypic tissue fabrication.* Trends in Biotechnology, 2011. **29**(4): p. 183-190.
10. Wang, Z., et al., *Fabricating Organized Elastin in Vascular Grafts.* Trends in Biotechnology.
11. Albrecht, D.R., et al., *Probing the role of multicellular organization in three-dimensional microenvironments.* Nature Methods, 2006. **3**(5): p. 369-375.
12. Bryant, S.J., et al., *Photo-patterning of porous hydrogels for tissue engineering.* Biomaterials, 2007. **28**(19): p. 2978-2986.
13. Tian, Z., et al., *Wave number–spiral acoustic tweezers for dynamic and reconfigurable manipulation of particles and cells.* Science Advances, 2019. **5**(5): p. eaau6062.
14. Chansoria, P., et al., *Ultrasound-assisted biofabrication and bioprinting of preferentially aligned three-dimensional cellular constructs.* Biofabrication, 2019. **11**(3): p. 035015.
15. Nguyen, T.D., et al., *Patterning and manipulating microparticles into a three-dimensional matrix using standing surface acoustic waves.* Applied Physics Letters, 2018. **112**(21): p. 213507.
16. Ozcelik, A., et al., *Acoustic tweezers for the life sciences.* Nature Methods, 2018. **15**(12): p. 1021-1028.
17. Li, P., et al., *Acoustic separation of circulating tumor cells.* Proceedings of the National Academy of Sciences, 2015. **112**(16): p. 4970-4975.
18. Zhang, S.P., et al., *Digital acoustofluidics enables contactless and programmable liquid handling.* Nature Communications, 2018. **9**(1): p. 2928.
19. Wu, M., et al., *Isolation of exosomes from whole blood by integrating acoustics and microfluidics.* Proceedings of the National Academy of Sciences, 2017.
20. Chen, Y., et al., *Rare cell isolation and analysis in microfluidics.* Lab on a Chip, 2014. **14**(4): p. 626-645.
21. Ahmed, D., et al., *Rotational manipulation of single cells and organisms using acoustic waves.* Nature Communications, 2016. **7**: p. 11085.
22. Li, S., et al., *Standing Surface Acoustic Wave Based Cell Coculture.* Analytical Chemistry, 2014. **86**(19): p. 9853-9859.
23. Yeo, L.Y. and J.R. Friend, *Surface Acoustic Wave Microfluidics.* Annual Review of Fluid Mechanics, 2014. **46**(1): p. 379-406.
24. Ding, X., et al., *Surface acoustic wave microfluidics.* Lab on a Chip, 2013. **13**(18): p. 3626-3649.
25. Fu, Y.Q., et al., *Advances in piezoelectric thin films for acoustic biosensors, acoustofluidics and lab-on-chip applications.* Progress in Materials Science, 2017. **89**: p. 31-91.
26. Guo, F., et al., *Reusable acoustic tweezers for disposable devices.* Lab on a Chip, 2015. **15**(24): p. 4517-4523.
27. Hodgson, R.P., et al., *Transmitting high power rf acoustic radiation via fluid couplants into superstrates for microfluidics.* Applied Physics Letters, 2009. **94**(2): p. 024102.
28. Witte, C., et al., *Microfluidic resonant cavities enable acoustophoresis on a disposable superstrate.* Lab on a Chip, 2014. **14**(21): p. 4277-4283.
29. Connacher, W., et al., *Micro/nano acoustofluidics: materials, phenomena, design, devices, and applications.* Lab on a Chip, 2018. **18**(14): p. 1952-1996.

30. Bourquin, Y., et al., *Tuneable surface acoustic waves for fluid and particle manipulations on disposable chips.* Lab on a Chip, 2010. **10**(15): p. 1898-1901.
31. Wilson, R., et al., *Phononic crystal structures for acoustically driven microfluidic manipulations.* Lab on a Chip, 2011. **11**(2): p. 323-328.
32. Reboud, J., et al., *Shaping acoustic fields as a toolset for microfluidic manipulations in diagnostic technologies.* Proceedings of the National Academy of Sciences, 2012. **109**(38): p. 15162-15167.
33. Bourquin, Y., et al., *Integrated immunoassay using tuneable surface acoustic waves and lensfree detection.* Lab on a Chip, 2011. **11**(16): p. 2725-2730.
34. Reboud, J., et al., *Nebulisation on a disposable array structured with phononic lattices.* Lab on a Chip, 2012. **12**(7): p. 1268-1273.
35. Shilton, R.J., et al., *Rotational microfluidic motor for on-chip microcentrifugation.* Applied Physics Letters, 2011. **98**(25): p. 254103.
36. Glass, N.R., et al., *Miniaturized Lab-on-a-Disc (miniLOAD).* Small, 2012. **8**(12): p. 1881-1888.
37. Tao, X., et al., *3D patterning/manipulating microparticles and yeast cells using ZnO/Si thin film surface acoustic waves.* Sensors and Actuators B: Chemical, 2019. **299**: p. 126991.
38. Nguyen, T.D., et al., *Acoustofluidic closed-loop control of microparticles and cells using standing surface acoustic waves.* Sensors and Actuators B: Chemical, 2020: p. 128143.
39. Spicer, C.D., *Hydrogel scaffolds for tissue engineering: the importance of polymer choice.* Polymer Chemistry, 2020. **11**(2): p. 184-219.
40. Antoine, E.E., P.P. Vlachos, and M.N. Rylander, *Review of collagen I hydrogels for bioengineered tissue microenvironments: characterization of mechanics, structure, and transport.* Tissue engineering. Part B, Reviews, 2014. **20**(6): p. 683-696.
41. Caliari, S.R. and J.A. Burdick, *A practical guide to hydrogels for cell culture.* Nature Methods, 2016. **13**: p. 405.
42. Murphy, S.V. and A. Atala, *3D bioprinting of tissues and organs.* Nat Biotech, 2014. **32**(8): p. 773-785.
43. Mandrycky, C., et al., *3D bioprinting for engineering complex tissues.* Biotechnology Advances, 2016. **34**(4): p. 422-434.
44. Bruus, H., *Acoustofluidics 2: Perturbation theory and ultrasound resonance modes.* Lab on a Chip, 2012. **12**(1): p. 20-28.
45. Isenberg, B.C. and J.Y. Wong, *Building structure into engineered tissues.* Materials Today, 2006. **9**(12): p. 54-60.
46. Holder, A.J., et al., *Control of collagen gel mechanical properties through manipulation of gelation conditions near the sol–gel transition.* Soft Matter, 2018. **14**(4): p. 574-580.
47. Chen, C., et al., *Three-dimensional numerical simulation and experimental investigation of boundary-driven streaming in surface acoustic wave microfluidics.* Lab on a Chip, 2018.
48. Doinikov, A.A., P. Thibault, and P. Marmottant, *Acoustic streaming in a microfluidic channel with a reflector: Case of a standing wave generated by two counterpropagating leaky surface waves.* Physical Review E, 2017. **96**(1): p. 013101.
49. Doinikov, A.A., P. Thibault, and P. Marmottant, *Acoustic streaming induced by two orthogonal ultrasound standing waves in a microfluidic channel.* Ultrasonics, 2018. **87**: p. 7-19.

50. Hamilton, M.F., Y.A. Ilinskii, and E.A. Zabolotskaya, *Acoustic streaming generated by standing waves in two-dimensional channels of arbitrary width.* The Journal of the Acoustical Society of America, 2003. **113**(1): p. 153-160.
51. Kiebert, F., et al., *3D measurement and simulation of surface acoustic wave driven fluid motion: a comparison.* Lab on a Chip, 2017. **17**(12): p. 2104-2114.
52. Darinskii, A.N., M. Weihnacht, and H. Schmidt, *Surface acoustic wave electric field effect on acoustic streaming: Numerical analysis.* Journal of Applied Physics, 2018. **123**(1): p. 014902.
53. Alghane, M., et al., *Experimental and numerical investigation of acoustic streaming excited by using a surface acoustic wave device on a 128° YX-LiNbO3substrate.* Journal of Micromechanics and Microengineering, 2010. **21**(1): p. 015005.
54. Kurashina, Y., et al., *Enzyme-free release of adhered cells from standard culture dishes using intermittent ultrasonic traveling waves.* Communications Biology, 2019. **2**(1): p. 393.